Fundamentals of Moisture Transport in Textiles

http://www.tfe.gatech.edu/beckham/C97-G31

Haskell W. Beckham, Johannes Leisen, H. Stephen Lee, Wallace W. Carr
School of Textile and Fiber Engineering
Georgia Institute of Technology, Atlanta, GA 30332-0295

Steven B. Warner, Esra Coskuntuna, Fred Kim
University of Massachusetts, Dartmouth, MA

PROJECT GOALS: To understand and quantify moisture transport in textile structures so that novel/improved materials for fluid management and novel/improved drying processes may be developed.

ABSTRACT

Magnetic resonance imaging (MRI) and other techniques are being used to investigate moisture transport in textiles. MRI revealed that moisture distribution in carpet is significantly influenced by the vacuum extraction procedure. Industrially relevant through-flow drying of carpet has been simulated on a laboratory through-flow dryer (LTFD) as well as inside a MRI scanner. The effects of the moisture distribution and the air flow direction on through-flow drying of unbacked tufted carpet are being studied. Methods to achieve faster drying via increased carpet air permeability are being developed. Based on experimental results obtained using LTFD, the potential to improve drying in constant rate and falling rate drying periods is being explored. Anisotropic wicking of fabrics is being studied. Two different types of fabrics with different wicking properties were designed and are being tested for the desired wicking properties.

INTRODUCTION

Innovative and improved manufacturing processes can only be developed if the interactions between process chemicals and textile products are understood on a fundamental level. For example, current drying processes can be made much more efficient, migration problems can be controlled, and completely new designs for drying equipment can be proposed. In addition, new materials for fluid management can only be developed by understanding fundamental interactions between fluids and fibrous assemblies.

While optical imaging methods are well-suited for the analysis of surface and transparent substrates, magnetic resonance imaging (MRI) readily provides 3D water distributions within opaque textile substrates. In this study, standard MRI techniques are being employed to measure

one-, two- and three-dimensional images of water within wet textile substrates. Because a single one-dimensional image can be measured in a matter of milliseconds, real-time monitoring of actual drying processes is possible. Mechanisms of drying are being established by following water distributions as a function of drying time.

Carpet air permeability is a very important parameter affecting drying time for through-air drying. Using a modified Frazier air permeability tester (FAPT) and a laboratory through-flow dryer (LTFD), we have studied the effects of several carpet construction and process parameters on air permeability of unbacked cut-pile nylon carpet with woven polypropylene primary backing. A model predicting pressure drop over the carpet versus apparent velocity was developed. The results indicate that woven primary backing section is the main resistance to airflow through the carpet. Modifications of the backing section that will increase carpet air permeability, and thus improve through-flow drying rates, are being studied.

Understanding lateral wicking behavior in textiles is necessary to control migration during drying processes, and to improve function in consumer products designed to transport fluids away from undesired areas. Thus, the effects of several construction parameters on the wicking properties are examined. Several mathematical models of anisotropic wicking in given fabric structures are developed.

The following sections describe the varied aspects of this multifaceted project. While MRI is one of the major tools, other methods are used where appropriate. Specific fibrous substrates are being chosen for examination if their structures can lend insight into the fundamentals of moisture transport in textiles. For example, despite the obvious technical importance of understanding drying mechanisms in cut-pile carpet, these materials also serve as simple model systems. The pile region consists of loosely packed fibers compared to the backing region. Hence, these carpets are ideally suited to study effects of fiber packing on capillary forces, moisture transport, and how these are affected by pressure and temperature variations.

MOISTURE DISTRIBUTION

Magnetic resonance imaging has been used to visualize moisture distribution in unbacked cut-pile nylon carpet following the dyeing process and after vacuum extraction. At moisture levels typical of those following laboratory hydro-extraction (i.e., ~50%), the water distribution within the carpet yarns depends on the vacuum direction. Figure 1 shows the moisture distribution when the excess water is removed by vacuum extraction from either the surface (Figure 1a) or the back (Figure 1b). When the surface is vacuumed, the water concentrates in the pile region, a distribution that is different from that observed when the sample is vacuumed from the back. Based on these results, the effects of moisture distribution on drying are discussed next.

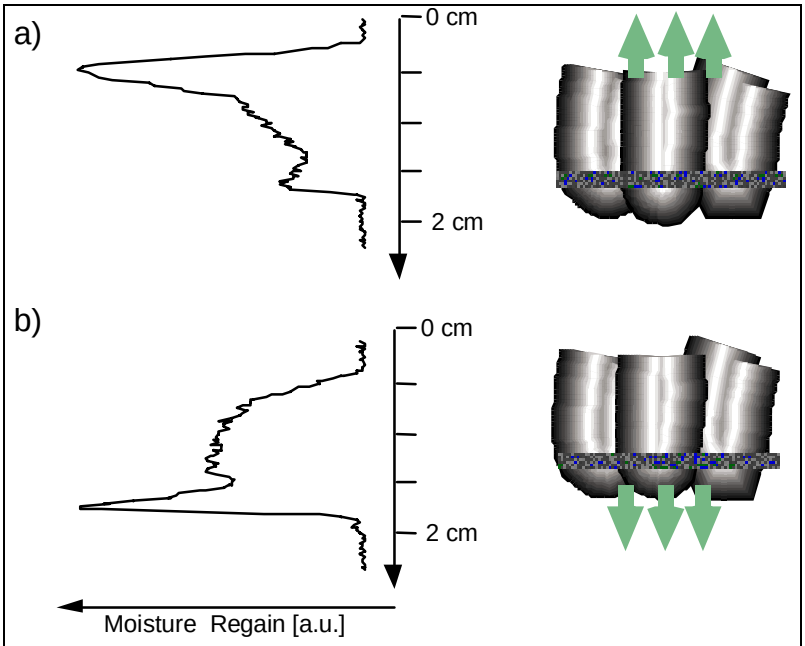

Figure 1. 1D profile images of water in a piece of cut-pile nylon carpet following vacuum extraction to bring the moisture regain to 50%. Extraction from: (a) top surface of carpet and (b) back of the carpet.

DRYING

Through-flow drying was simulated inside the MRI scanner. Moisture profiles as a function of drying time were measured for air entering either the top surface or the back of the carpet. Integration over the measured spatial water profile provides the overall moisture regain as a function of time.

Sample sizes are limited within our MRI scanner (≤ 1-inch diameters). It is important to be able to compare our experiments with data collected on larger samples to ensure that meaningful conclusions are drawn. For this purpose a laboratory through-flow dryer has been designed and constructed (cf. Figure 2). This apparatus allows the observation of drying processes on circular carpet samples with 1-foot diameters. Many parameters such as air temperature, flow rate and relative humidity can be controlled to simulate a wide variety of industrial drying conditions. The actual moisture regain is monitored gravimetrically by observing the weight loss as a function of drying time.

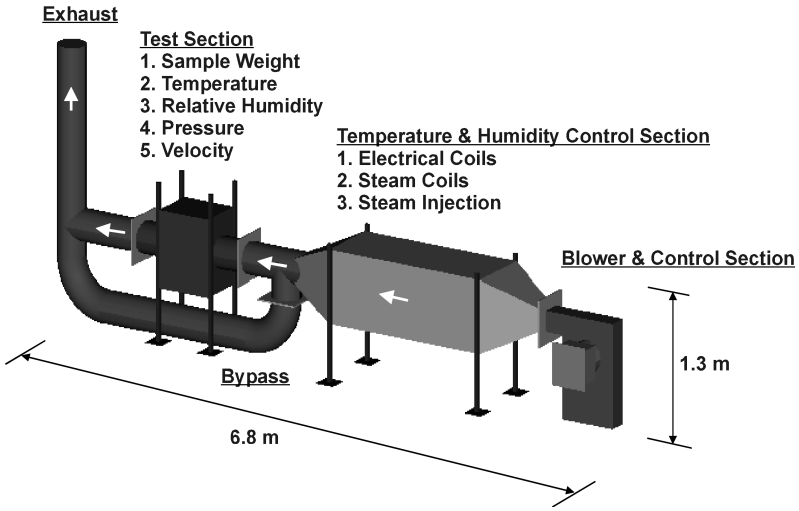

Figure 2. Experimental setup to simulate industrial drying processes on textiles. Parameters such as airflow rate, moisture regain and relative humidity can be varied.

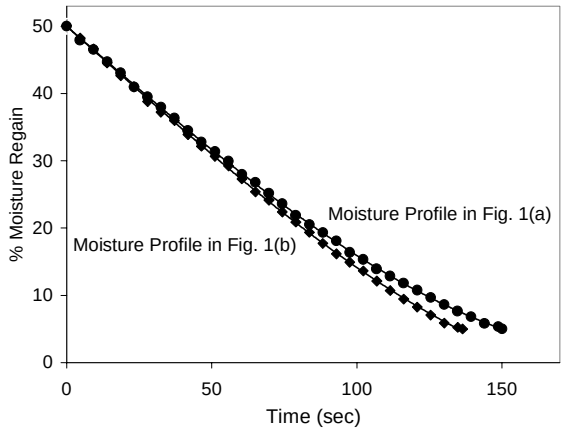

Figure 3. Moisture regain during the drying process for different beginning moisture profiles in Figure 1.

Effects of Moisture Distribution on Drying

Since moisture distribution may vary with vacuum procedure, the effects of moisture distribution on drying have been conducted. The results for drying at an air temperature of 80 °C and an air flow rate of 30 m/min are shown in Figure 3. Carpet with water concentrated in the front of the pile region (Figure 1a) dries slightly slower than when the water is concentrated more towards the primary backing (Figure 1b).

Effects of Flow Direction on Drying

Since in industrial through-flow dryers air may enter either the carpet face or the back, the effect of flow direction on drying was studied using MRI and LTFD. As shown in Figure 4, when air enters the carpet back, pile and backing regions reach the same low moisture levels at the same time. When air enters the carpet surface, the pile region dries faster than the backing region. For both flow directions, a significantly faster moisture loss for the backing region is observed (which initially contains the higher moisture concentration). For the air flow entering the surface, after 10 minutes a sufficiently low moisture content is reached for the pile region, while at this time still more than 40% moisture is present in the backing region. However, overall drying rate did not depend on flow direction. This was confirmed by a number of drying tests for several styles of carpets at different air temperatures (25~116 °C) and air flow rates (20~30 m/min).

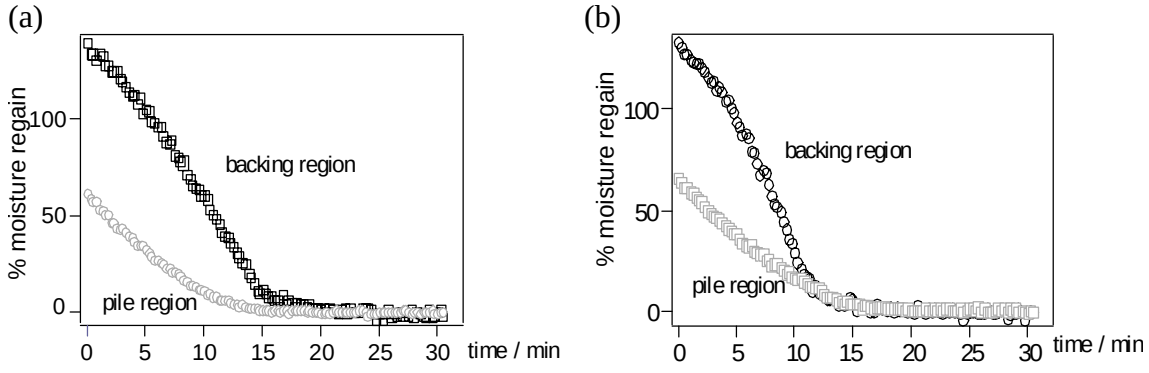

Figure 4. Moisture regain during the drying process in the pile and backing regions: (a) air flow entering surface, (b) air flow entering back at room temperature and flow rate (20 m/min).

Faster Drying via Increased Carpet Air Permeability

Woven polypropylene primary backing has been widely used in the tufted carpet manufacturing process for three decades. Since drying rate depends greatly on air velocity, carpet air permeability is a very important parameter affecting drying time. A modified FAPT and LTFD were used to study the effects of several carpet construction and process parameters on air permeability of unbacked cut-pile nylon carpet with woven polypropylene backing. Although several parameters affected air permeability, by far, the most significant parameter was weft density of the primary backing. Also, the results indicated the woven backing section, the primary backing and yarns tufted through it, was the main resistance to airflow through the carpet. Thus, techniques to increase air permeability of this section without adversely affecting carpet properties are being investigated since an increase in air permeability should increase the drying rate.

Since the primary backing greatly affects air permeability, nonwoven polyester backing was compared with woven polypropylene backing. Two unbacked tufted carpets with identical construction parameters except two different backing materials were tested. The air permeability for the carpet with nonwoven backing was significantly higher (See Figure 5a). As shown in Figure 5b for constant pressure drop across the carpet, the time required to dry the carpet with nonwoven backing to a moisture regain of about 5% was about one half that of the carpet with woven backing.

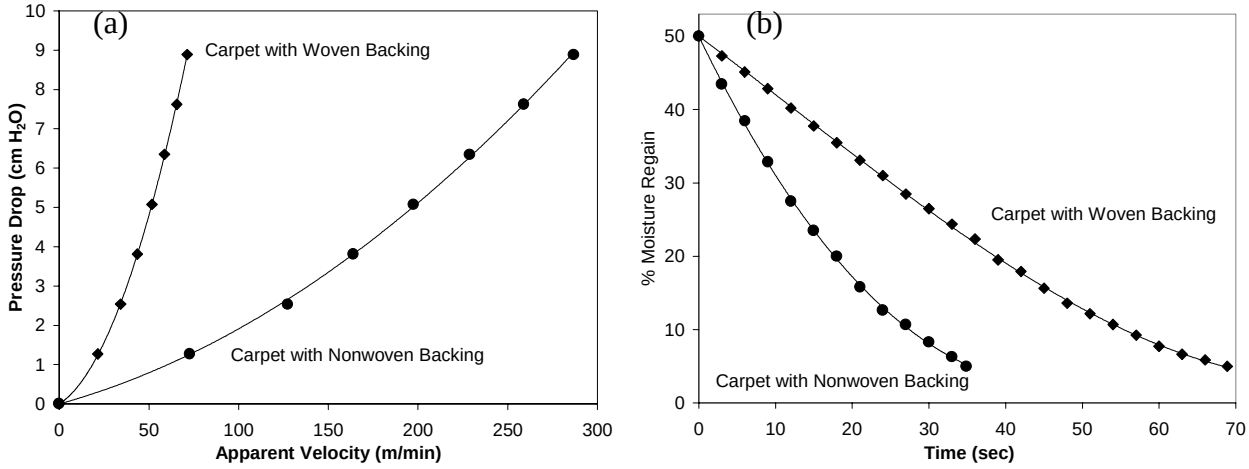

Figure 5. (a) Pressure drop vs apparent velocity for the two carpets with woven and nonwoven backings at standard conditions using the modified FAPT. (b) Moisture regain during the drying process at an air temperature of 116 °C and a pressure drop of 1.27 cm H_2O using LTFD.

Potential to Improve Through-flow Drying

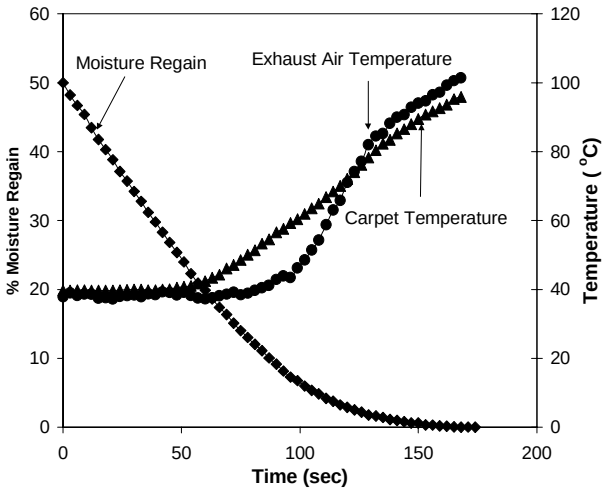

Figure 6. Moisture regain and temperature versus time for carpet sample Q5* during drying at an air temperature of 116 °C and a pressure drop of 2.03 cm H_2O across the carpet.

* Q5 is the unbacked cut-pile nylon carpet with an areal density of 1560 kg/m^2, a tufting density of 18 stitch/cm^2, and a pile height of 6.9 mm.

Figure 6 shows the variations of exhaust air and carpet temperatures for carpet sample Q5* during through-flow drying using LTFD. In the constant rate drying period (moisture regain over 20%), exhaust air temperature is about 40 °C, which is just slightly above the adiabatic saturation temperature of 37 °C of the air entering the carpet. This indicates that the exhaust air is almost saturated and the drying process is very effective in this period. Techniques, such as applications of acoustics, to increase heat and mass transfer rates should not be expected to increase drying rate in this period. On the contrary, during the falling rate drying period (moisture regain below 20%), the exhaust air temperature is significantly higher than the adiabatic saturation temperature, indicating that the through-flow drying process is much less effective in this period. Thus, research to increase effectiveness of through-flow drying of carpet should be focused on the region where the moisture regain of the carpet is between 5~20%.

ANISOTROPIC WICKING

Two different types of fabrics were designed to give desired wicking properties. One type of fabric is a three-layer structure designed to rapidly transport in one direction with minimum wicking in any other direction. The other type was designed to wick liquid through the surface plane with minimum wicking in the plane of the fabric.

The first type of fabric consists of a layer of continuous filaments laid parallel to each other in between two layers of a thin nonwoven fabric. Continuous filaments are laid parallel to each other in the middle layer to maximize the fiber orientation in order to promote liquid flow in

that direction. The deniers of the continuous filaments are changed to quantify their effects on the rate of fluid flow. The layers will be held together by placing them between two glass plates. The distance between the glass plates is changed to vary the thickness of each sample.

For this type of structure, a polyester nonwoven fabric of unit weight 40 g/m^2 and thickness 34 mils is used for the top and bottom layers. This fabric is used in all samples so that the effects of the variables of the middle layer can be observed. Continuous filaments of 1500 denier and 185 denier are used for the middle layer. Two different 1500 denier yarns are used, one with 384 filaments and the other with 250 filaments. The 185 denier yarn has 36 filaments. The structures are tested to observe the distance the liquid travels with time in the axial and transverse directions.

The second type of fabric, which wicks liquid through the surface plane with minimum wicking in the plane of the fabric, is designed as a four-layer structure. The top and bottom layers are random laid nonwoven fabrics. These two layers are used as substrates in flocking. On these substrates, fibers are flocked to produce channels perpendicular to the surface of the fabric, enhancing the flow in the vertical direction. These channels are designed to promote the flow through the plane of the fabric, thus, minimizing the radial flow in the plane of the fabric. Two flocked layers are placed on top of each other with the flocked fibers facing each other. The flocking density and the denier of the fibers are varied to observe the effects of these variables in this structure.

For this type of structure, the fabric used for the substrates is a spunbonded nonwoven fabric with 4 denier straight continuous filaments PET. The unit weight of the fabric is 34 g/m^2, and its thickness is 0.36 mm. Nylon fibers of 3 denier and 20 denier are flocked on the substrates at two different flock densities. These samples are tested to observe how much of the liquid dropped is transferred to the bottom layer by measuring the distance the liquid travels in the top and bottom layers. The results of these tests will be used to model wicking in these structures.

Fluid motion in porous media can be described by the continuity equation for incompressible flow,

$$\nabla \cdot v_o = 0 \tag{1}$$

and Darcy's Law,

$$v_o = \frac{-k \cdot \nabla P}{\mu} \tag{2}$$

where k is the permeability, v_o is the apparent velocity of the fluid, P is the driving pressure for fluid motion, and μ is the viscosity of the fluid.

These equations can be solved to predict the radial in-plane movement of a liquid front in a fibrous network. The solution procedure is solving $\frac{\partial^2 P}{\partial x_1^2}+\left(\frac{k_2}{k_1}\right)\frac{\partial^2 P}{\partial x_2^2}=0$ for pressure distribution and substituting pressure distribution into Darcy's Law to yield superficial velocity.

This procedure results in an ordinary differential equation that predicts the temporal advancement of the liquid boundary. The differential equations describing the motion of the fluid front obtained by this method are as follows:
For the anisotropic case,

$$\frac{d\xi_f}{dt}=\frac{k_1\Delta P}{\varepsilon\mu R_o^2}\left[\frac{1}{1-\alpha}\right]\frac{1}{\left(\xi_f-\xi_o\right)\left(\cosh^2\xi_f-\cos^2\eta\right)} \tag{3}$$

where ξ_f is an elliptical extent and η is the elliptical equivalent of the in-plane angle. When the medium is anisotropic, the moving flow front is elliptic and is characterized by the maximum and the minimum radial extents R_{f1} and R_{f2}. Principal flow directions are x_1 and x_2, and they are orthogonal.

In the principal flow directions, the relation between radial extents and elliptical extents is

$$\xi_{f1}=\sinh^{-1}\left[\frac{R_{f1}}{R_o}\left(\frac{1}{1-\alpha}\right)^{-1/2}\right] \tag{4}$$

$$\xi_{f2}=\cosh^{-1}\left[\frac{R_{f2}}{R_o}(1-\alpha)^{-1/2}\right] \tag{5}$$

The elliptical equivalent of the inlet hole radius is

$$\xi_o=\ln\left[\frac{1+\alpha^{1/2}}{(1-\alpha)^{1/2}}\right]. \tag{6}$$

Using the initial condition, $\xi_f=\xi_o$ at $t=0$, the solution to the differential equation is found to be:

$$F(\xi_f,\eta)=\left(\xi_f-\xi_o\right)\left(\frac{\sinh(2\xi_f)}{4}+\frac{\xi_f}{2}\right)+\cos^2\eta\left(\xi_f\xi_o-\frac{\left(\xi_f^2+\xi_o^2\right)}{2}\right)+\left(\frac{\cosh(2\xi_o)-\cosh(2\xi_f)}{8}\right)$$
$$+\frac{\left(\xi_o^2-\xi_f^2\right)}{4}=\left[\frac{\alpha}{1-\alpha}\right]\Phi$$

where Φ is based on k_1, the maximum in-plane permeability.

The left-hand side of this equation will be determined from the experimental data. When F versus time is plotted, the slope of the line will be $m_\xi = \frac{k_1 \Delta P}{\varepsilon \mu R_o^2}\left[\frac{\alpha}{1-\alpha}\right]$. In this equation, μ is known, ΔP and ε are theoretically calculated knowing the geometry of the structure and R_o is determined experimentally.

For the second type of fabric, the model will be setup to predict the effects of the denier of the flock fibers and the flock density. In these models, it will be assumed that in fabric type 1, the middle layer, which consists of parallel-laid continuous filaments, and in fabric type 2, the middle layer that consists of the flocked fibers, dominate the directional permeability of the fabric structures.

REFERENCES

1. Callaghan, P. *Principles of Nuclear Magnetic Resonance Microscopy*; Clarendon: Oxford, 1991.
2. Blümich, B.; Kuhn, W., Ed.;*Magnetic Resonance Microscopy*; VCH-Verlagsgesellschaft: Weinheim, 1992.
3. Talagala, S. L.; Lowe, I. J. *Concepts in Magnetic Resonance* **1991**, *3*, 145.
4. Xia, Y. *Concepts in Magnetic Resonance* **1996**, *8*, 205.
5. Gladden, L. F. *The Chemical Engineering Journal* **1995**, *56*, 149.
6. Maneval, J. E.; In *Annual Reports on NMR Spectroscopy* ; Webb, G. A., Belton, P. S. and McCarthy, M. J., Ed.; Academic Press: New York, 1995; Vol. 31, 345.
7. Maneval, J. E., McCarthy, M. J., Whitaker, S.; In *Drying '91* ; Mujumdar, A. S. and Filková, I., Ed.; Elsevier Science: Amsterdam, 1991; Vol. , 170.
8. Carr, W. W., Tincher, W. C. *Textile Research Journal* **1983**, 219.
9. O'Dell, D. R., Carr, W. W. *Textile Research Journal* **1996**, *66*, 366.
10. Adams *et al*., *Textile Research Journal* **1987**.

PUBLICATIONS

11. Lee HS, Carr WW, Beckham HW, Wepfer WJ, “Factors Influencing the Air Flow Through Unbacked Tufted Carpet”, submitted to *Textile Research Journal*, 5 August **1999**.
12. Leisen J, Beckham HW, Good J, Warner S, Carr WW, ”Magnetic Resonance Imaging of Water Ingress and Distribution in Fluorochemical-Finished Polyester Cut-Pile Carpet”, *Textile Chemist and Colorist* **1999**, *31(4)*, 21-26.
13. Leisen J, Hou L, Beckham HW, Carr WW, "Observation of the Water Distribution during Drying of Textiles", In Spatially Resolved Magnetic Resonance: Methods, Materials, Medicine, Biology, Rheology, Geology, Ecology, Hardware, P. Bluemler, B. Bluemich, R. Botto, E. Fukushima, Eds., Viley-VCH **1998**.

14. Beckham HW, Fülber C, Spiess HW, Blümich B, “Nuclear Magnetic Resonance Imaging of Water Distributions in Loop-Pile Nylon Carpet Tile", *J. Text. Inst., Pt 1* **1998**, *89(2)*; 436.
15. Zhou W, Warner S, “Pore Sizes in Carpet”, *Textile Research Journal* **1998**, in press.
16. Beckham HW, Leisen J, Carr WW, “Magnetic Resonance Imaging of Water Distribution in Carpet” AATCC Book of Papers, **1997** International Conference & Exhibition.

PRESENTATIONS

17. Leisen, J, Beckham HW, “Magnetic Resonance Imaging of Fluids in Nonwovens” 9th annual TANDEC NONWOVENS Conference; Knoxville/ TN; 10-12 November **1999**.
18. Leisen J, Beckham HW, Hojjatie B, Doffin D, “Quantitative Application of Magnetic Resonance Microscopy for the Characterization of Moisture Distributions in Fibrous Substrates”, 5th International Conference on Magnetic Resonance Microscopy; Heidelberg, Germany; 5-9 September **1999**.
19. Leisen J, Kinser H, Beckham HW, “Fluid Distribution and Diffusion in Engineered Fibrous Substrates via Diffusion NMR and NMR Imaging”, 218th ACS national meeting; New Orleans, LA; 21-26 August **1999**.
20. Lee HS, Carr WW, Leisen, J, Beckham HW, “Observation and Simulation of Heat and Moisture Transport during Through-Air Drying of Cut-Pile Tufted Carpet”, the 12th Annual Polymer Education & Research Review Meeting; Atlanta, GA; June **1999**.
21. Lee HS, Carr WW, Leisen, J, Beckham HW, “Observation and Simulation of the Industrial Through-Air Drying Process for Cut-Pile Tufted Carpet”, the 4th Annual Conference on Recycling of Fibrous Textile and Carpet Waste; Dalton, GA; May **1999**.
22. Beckham HW, Leisen J, Carr WW, "Magnetic Resonance Imaging of Moisture in Textiles", Nonwovens Conference, Proceedings of TAPPI; Orlando, FL; 20-24 April **1999**.
23. Beckham HW, "Magnetic Resonance Imaging of Fluids in Textiles”, Fachhochschule Niederrhein; Krefeld, Germany; 18 June **1998**.
24. Leisen J, Beckham HW, Carr WW, “Observation of Drying Processes in Textiles by Magnetic Resonance Microscopy”, 39th Experimental NMR Conference; Pacific Grove, CA; 22–27 March **1998**.
25. Beckham HW “Magnetic Resonance Imaging of Water Distribution in Carpet: Drying Studies” AATCC International Conference & Exhibition; Atlanta, GA; 29 September **1997**.
26. Leisen J, Beckham HW, Carr WW “Observation of Water Distribution and Diffusion during the Drying Process in Textiles” 4th International Conference on Magnetic Resonance Microscopy and Macroscopy; Albuquerque, NM; 21–25 September **1997**.
27. Beckham HW, “Magnetic Resonance Imaging of Fluids in Engineered Fibrous Substrates” DuPont; Chattanooga, TN; 19 September **1997**.